

A ghost mechanism: An analytical model of abrupt learning

Fatih Dinc,^{1,2,*} Ege Cirakman,^{1,*} Yiqi Jiang,¹ Mert Yuksekgonul,³ Mark Schnitzer,^{1,4,5,†} and Hidenori Tanaka^{2,6,†}

¹*CNC Program, Stanford University, Stanford, CA 94305, USA*

²*Physics & Informatics Laboratories, NTT Research Inc., Sunnyvale, CA 94085, USA*

³*Computer Science, Stanford University, Stanford, CA 94305, USA*

⁴*James H. Clark Center for Biomedical Engineering & Sciences, Stanford University, Stanford*

⁵*Howard Hughes Medical Institute, Stanford University, Stanford, CA 94305, USA*

⁶*CBS-NTT Program in Physics of Intelligence, Harvard University, Cambridge, MA 94305, USA*

Abrupt learning is commonly observed in neural networks, where long plateaus in network performance are followed by rapid convergence to a desirable solution. Yet, despite its common occurrence, the complex interplay of task, network architecture, and learning rule has made it difficult to understand the underlying mechanisms. Here, we introduce a minimal dynamical system trained on a delayed-activation task and demonstrate analytically how even a one-dimensional system can exhibit abrupt learning through ghost points rather than bifurcations. Through our toy model, we show that the emergence of a ghost point destabilizes learning dynamics. We identify a critical learning rate that prevents learning through two distinct loss landscape features: a no-learning zone and an oscillatory minimum. Testing these predictions in recurrent neural networks (RNNs), we confirm that ghost points precede abrupt learning and accompany the destabilization of learning. We demonstrate two complementary remedies: lowering the model output confidence prevents the network from getting stuck in no-learning zones, while increasing trainable ranks beyond task requirements (*i.e.*, adding sloppy parameters) provides more stable learning trajectories. Our model reveals a bifurcation-free mechanism for abrupt learning and illustrates the importance of both deliberate uncertainty and redundancy in stabilizing learning dynamics.

Understanding the mathematical principles that govern learning dynamics is crucial for advancing the frontiers in both natural and artificial neural networks [1–8]. Empirically, networks often learn to internalize the structure of tasks and exhibit sudden drops in their loss function, which mark the acquisition of new computational capabilities [9–19]. Such abrupt transitions frequently accompany instabilities in learning dynamics, including exploding or vanishing gradients and abrupt shifts in network behavior [20–22]. While a variety of prior works exhibits slow learning followed by sudden performance jumps [23, 24], the precise mechanisms underlying this phenomenon remain poorly understood.

One recent productive approach in this direction involves using dynamical systems theory to study RNNs through the lens of dynamical systems theory [25–32]. During training, RNNs often show destabilized gradients, leading to well-documented learning instabilities [9, 20, 21, 33, 34]. Analysis of RNNs’ attractor landscapes [9, 11, 25, 34–36] has identified bifurcations (*i.e.*, shifts in system behavior, which alter the number or stability of fixed points, periodic orbits, or other invariant sets [33, 37–43]) as key events facilitating the acquisition of novel capabilities [9, 11]. Traditional work in dynamical system theory has established several mechanisms that support robust system behavior without originating from bifurcations. For instance, ghost points, where state variables change very slowly (unlike fixed-points where no change occurs) [37], can help track time. Therefore, limiting the analysis of learning dynamics to bifurcations may overlook important processes that drive abrupt learning.

We start this letter by illustrating the sudden learning phenomenon using a simple example with recurrent neural networks (RNNs). In this “*delayed-activation task*,” networks are initialized to a specific state and must output zero for a delay period, T , after which the output is expected to “activate” and become one. As discussed in **End Matter**, (low-rank [28]) RNNs trained on this task exhibit abrupt learning, where long plateaus in loss value are followed by rapid convergence. To study this phenomenon systematically, we introduce an analytically tractable one-dimensional dynamical system trained on the delayed-activation task and demonstrate how this system exhibits abrupt learning despite its simplicity. Through analysis of this system, we identify a novel mechanism underlying abrupt learning without bifurcations, characterized by the rapid emergence of ghost points (approximate saddle points [37]). Next, we demonstrate that RNNs’ learning dynamics can be substantially stabilized by artificially reducing the confidence level of their outputs and increasing the number of trainable ranks. The former observation underscores the importance of secondary, not goal-directed, mechanisms to stabilize learning, whereas the latter has implications for learning dynamics in low-rank RNNs [28–32]: The presence of “sloppy” (*e.g.*, randomly connected) ranks, which may not necessarily be part of the computation in the fully trained (effectively low-rank) RNNs [29, 32], may support stable learning dynamics.

Our toy model (Fig. 1) is a one-dimensional dynamical system that follows the prototypical form of the saddle-node bifurcation ($\dot{x} = x^2 + r$, [37]). Here, $x \in \mathbb{R}$ is the scalar state variable and $r \in \mathbb{R}$ is the *learnable* parameter.

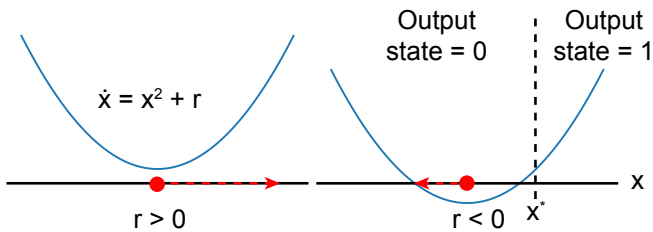


FIG. 1. **Visualization of the toy model with a single dynamical variable undergoing a saddle-node bifurcation.** We initialize the variable at $x(0) = 0$ (red dot). *Left.* For $r > 0$, the system evolves towards $x \rightarrow \infty$ (red arrow). *Right.* For $r < 0$, the system evolves towards a fixed point at $-\sqrt{-r}$. A pre-defined x^* divides the model output into two states.

This toy model has two fixed points (*i.e.*, where $\dot{x} = 0$) for $r < 0$, and none for $r > 0$. The change in the number of fixed points at $r = 0$ signals a saddle-node bifurcation [37]. This phenomenon has been well studied by varying r and drawing bifurcation diagrams [37], but not within the context of loss minimization. In this work, we take the latter approach and *train* the dynamical system to learn a delayed-activation (DA) task.

In the DA task, we set the initial condition with $x(0) = 0$, and define the model output as $\hat{o}(x) = \sigma(c(x - x^*))$, where $x^* > 0$ and $c > 0$ are pre-defined constants, and σ is the sigmoid function. In the limit $c \rightarrow \infty$, this output confidently takes on binary values, either 0 or 1, hence we call c the “confidence” parameter. The objective of the task is for the toy model’s output ($\hat{o}(x(t))$) to match the target output ($o(t)$) of 0 until some pre-defined time point $t < T$, and transition to 1 for $T < t < 2T$. Since the only learnable parameter is r , the learning process should pick an optimal value, r^* , to ensure this condition. We achieve this goal by minimizing a loss function:

$$\mathcal{L}(r) = \int_0^{2T} (\hat{o}(x(t)) - o(t))^2 dt. \quad (1)$$

As we show in **End Matter**, in the analytical limit ($x^*, c \rightarrow \infty$), the loss function can be calculated as:

$$\mathcal{L}(r) = \begin{cases} \left| T - \frac{\pi}{2\sqrt{r}} \right| & \text{for } r \geq \frac{r^*}{4}, \\ T & \text{otherwise.} \end{cases} \quad (2)$$

Here, $r^* = \frac{\pi^2}{4T^2}$ is the optimal value, which is small but nonzero for large T . For the optimal parameter, the state variable ($x(t)$) lingers around the origin with negligible changes up to T , before abruptly shooting off to ∞ . Even though the toy model has no fixed points for $r^* > 0$ (and thus for any T), the origin resembles one ($\dot{x} \approx 0$) for times $t \ll T$ and is therefore termed as a “ghost” in the traditional literature [37]. Yet, for large T , r^* may become smaller than the precision of numerical fixed point finders, which would therefore be unable to distinguish

the ghost from a fixed point [25, 44]. Below, we rely on analytical tools instead.

As a first step, we set out to gain qualitative insights for whether loss minimization with a gradient-based method would succeed. To do so, we plotted Eq. (2) and numerically calculated loss function values (with finite x^*, c) with respect to r in Fig. 2A, which revealed three unique insights: (1) For any $r < r^*/4$, loss minimization would enter a no-learning zone and cannot easily recover due to flat loss function values, *i.e.*, zero gradients ($\nabla \mathcal{L}(r < r^*/4) = 0$) in the analytical limit. We call the boundary of this regime, $r = r^*/4$, as the “point of no return.” (2) Though r^* is a global minimum, the gradient is discontinuous at $r = r^*$, *i.e.*, $\nabla \mathcal{L}(r \rightarrow r^*)$ does not exist. As we discuss in **End Matter**, this would lead to oscillatory behavior near the minimum, which implies the existence of a maximum learning rate for a naive gradient descent approach (*i.e.*, updates of the form $r \rightarrow r - \alpha \nabla \mathcal{L}(r)$, where α is the learning rate), beyond which learning stops: $\alpha^* = \frac{3\pi^4}{32} T^{-5}$. For any $\alpha \geq \alpha^*$, the training process would eventually enter the no-learning zone (where gradients are exactly zero in the limit $c \rightarrow \infty$) and can no longer recover. (3) Picking the learning rate close to α^* is necessary to achieve learning as the loss function quickly saturates to flat values, *i.e.*, $\mathcal{L}(r) \rightarrow T$ for large $r \gg r^*$. Since the loss function also changes abruptly for $\frac{r^*}{4} < r < r^*$ (between 0 and T), minimizing it would lead to a abrupt decline as r approaches r^* .

To verify these theoretical insights, we conducted optimization experiments with naive gradient descent and fixed learning rates (Fig. 2B-D), where a single epoch corresponds to a numerical update with the analytically computed gradient (**End Matter**). Starting the training from $r = 10r^*$ and using a learning rate $\alpha < \alpha^*$, we observed a abrupt decay of loss function values around epoch 1500, followed by oscillations near the global optimum (Fig. 2B-C). In contrast, picking a larger learning rate, $\alpha > \alpha^*$, pushed the network into the no-learning zone (Fig. 2B-C). Moreover, varying the learning rate values confirmed that there was indeed a maximum learning rate, α^* , beyond which learning did not take place (Fig. 2D). Even though smaller learning rates led to lower final errors, learning within few epochs was only achieved with learning rates close to criticality, $\alpha \approx \alpha^*$. Finally, since r values are always positive during learning, the abrupt decays in Fig. 2B-C are not preceded by bifurcations. This observation showcases an alternative mechanism (here, emergence of ghost points) for acquiring novel capabilities in task-trained dynamical systems. Interestingly, even though a global minimum with zero loss value exists, the toy model cannot easily attain it using gradient descent due to complex learning dynamics (Fig. 2). While learning instabilities are expected in deep learning models solving complex tasks [45], here, a simple toy model with just one state variable and one

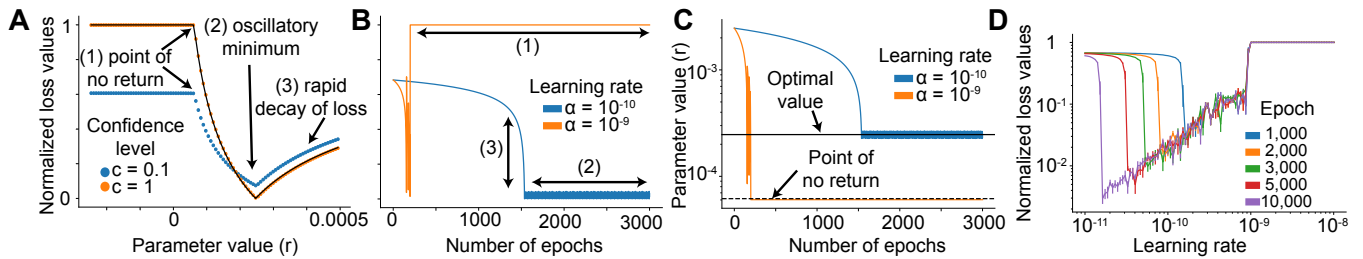


FIG. 2. **Our toy model trained on the delayed-activation task captures abrupt learning dynamics phenomena.** **A** We compared the analytical loss function (black line) vs those computed from realistic parameters (colored dots), in which the model output was defined via a sigmoid function $\hat{o}(x) = \sigma(c(x - x^*))$. The loss function had three distinct regimes: (1) a point of no return, (2) a minimum with non-zero gradient, and (3) abrupt decay of the loss function for $r \geq r^*$, where $r^* = \frac{\pi^2}{4T^2}$ is the global minimum. Parameters: $T = 100$, $\Delta t = 0.1$, and $x^* = 10$. **B-C** Initializing at $r := 10r^*$, we minimized the loss function values using gradient descent with different learning rates, recapitulating all three regimes in learning dynamics. Notably, for $\alpha = 10^{-10}$, even though the loss function decrease abruptly around epoch 1500, the network does not undergo any bifurcations, as evident from r not changing its sign during learning. **D** The toy model learned best with lower learning rates, but at the expense of more epochs of training. As predicted by the theory, learning is no longer possible for $\alpha \geq 9 * 10^{-10}$. Solid lines: means. Error bars: s.e.m. over 10 training instances, in which r was initialized following a normal distribution that has the mean $10r^*$ and the standard deviation $\frac{r^*}{10}$. Parameters for (b-d): $T = 100$ and $x^*, c \rightarrow \infty$ (analytical model).

parameter successfully captures several complex learning behaviors commonly observed in practice, such as oscillatory minima (see blue lines in Fig. 2B-C) and a range of effective learning rates (Fig. 2D). Thus, our toy model in Fig. 1 may constitute a simple yet useful testbed for future research into learning dynamics.

Next, we set out to apply the insights we learned from our toy model to study the learning dynamics in RNNs. Specifically, we conjectured that RNNs may acquire new capabilities through bifurcation-free mechanisms. Moreover, the observation of learning instabilities in low-dimensional dynamical systems may have practical implications for recent research focused on low-rank RNNs. Specifically, previous research has shown that training RNNs (with many parameters, *e.g.*, $W \in \mathbb{R}^{N \times N}$ for some large N) often leads to effectively low-rank updates after training is completed [29, 32]. However, this can occur following two distinct strategies of parameter changes: (1) updates may be performed across all dimensions and then gradually refine the parameters into a final low-rank structure, or (2) updates may be restricted to low-rank components from the outset, as in FORCE learning [46] and/or traditional low-rank RNN training [28, 31]. Below, we refer to these training strategies (1) and (2), respectively.

Since the strategy (2) is equivalent to training low-dimensional systems (see Eq. (4) below), we predicted that this strategy may face similar learning instabilities as those seen with our toy model. To investigate these predictions, we next studied the learning dynamics in low-rank RNNs (with many tunable parameters) trained to solve the DA task. Specifically, we focused on a simple, yet powerful, class of RNNs with the following equations

[47]:

$$\tau \dot{x}(t) = -x(t) + \tanh(Wx(t) + b), \quad (3)$$

where $x(t) \in \mathbb{R}^N$ are firing rates of N neurons, τ is the neuronal decay time, $W \in \mathbb{R}^{N \times N}$ and $b \in \mathbb{R}^N$ are the trainable weights and biases. Here, we first focus on rank-one RNNs, in which W is constrained to have $N - 1$ zero singular values. These RNNs are theoretically capable of solving the DA task due to their universal approximation property [31]. However, existing work makes no prediction about their learning dynamics.

To fill this gap and study the learning dynamics, we enforce the rank constraint by constructing $W = mn^T$ for $m \in \mathbb{R}^N$ and $n \in \mathbb{R}^N$. Using this relationship, we can define a latent variable, $\kappa(t) = n^T x(t)$, such that the RNN equations transform into a one-dimensional form:

$$\tau \dot{\kappa}(t) = -\kappa(t) + n^T \tanh(m\kappa(t) + b) = f(\kappa; m, n, b), \quad (4)$$

which we refer to as the latent circuit. In this transformed picture, training the RNN will implicitly update the parameters of the low-dimensional circuit, leading to the learning of any desired flow dynamics ($f(\kappa; m, n, b)$) [31]. We do not enforce any constraints on this dynamical system, only that the RNN should be optimized to solve the DA task, where we define the output as:

$$\hat{o}(\kappa) = \sigma(c(\kappa - \kappa^*)), \quad (5)$$

for some κ^* , and once again minimize the difference between $o(t)$ and $\hat{o}(\kappa(t))$. As we do so, we can use the learned parameters (m, n, b) and Eq. (4) to visualize the latent dynamical system emerging from the training.

As a first step, we confirmed that rank-one RNNs can learn the DA task (Fig. S1). Notably, training RNNs reproduced the same dependence on the learning rate as

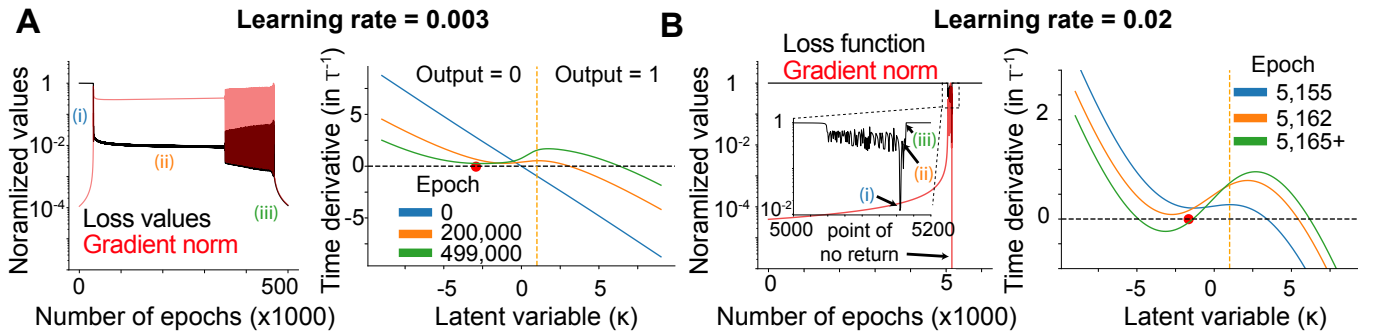


FIG. 3. A rank-one RNN trained on the delayed-activation task reproduced the main findings of the toy model. We trained a rank-one RNN on the DA task, in which the output of the RNN was defined as $\hat{o}(\kappa) = \sigma(c(\kappa - 1))$. Here, κ is the latent variable and c is the confidence level. **A** The RNN trained with a relatively low learning rate showed the abrupt jump in the loss function (between (i) and (ii)), and had oscillatory behavior before converging to a minimum (between (ii) and (iii)). The resulting network learned local ghost points with a small, but non-zero, distance from the $y = 0$ line. **B** When training the same network with higher learning rate, a saddle-node bifurcation occurred, putting the network beyond the point of no return. The network could no longer recover, as indicated by the practically zero gradient after the bifurcation. Parameters: $\tau = 10ms$, $\Delta t = 5ms$, $T = 100ms$, $N = 100$ neurons, $c = 10$. We initialized all units to be $x(0) = -0.3$ and used stochastic gradient descent. Red dots correspond to the initial values of $\kappa(t)$ for the final networks.

was the case for the toy model (compare Figs. 2D and S1). Next, we reverse-engineered an RNN trained with a suitable learning rate (Fig. 3A). We observed the emergence of a (local) ghost point (Fig. 3A), which proceeded sharp transitions in both the loss function (abrupt decay) and the L_2 norm of the gradient (abrupt increase). Importantly, the latent variable near the ghost point had very slow time-dynamics, leading to slow changes in latent activations. By finetuning the distance at the ghost point (similar to r in our toy model above), RNN learns to wait for a delay period of T and output one only after the latent variable escapes the ghost point. When we studied the development of this ghost point in the latent circuit, we uncovered that the latent dynamical system has always had one fixed point (there was only one fixed point after every epoch within $\kappa \in [-15, 15]$; data not shown). Consequently, as in our toy model, this RNN created the ghost point without undergoing a bifurcation.

Similar to the toy model, the learning dynamics in RNNs also showed the oscillatory behavior for low loss function values (Fig. 3A). Yet, unlike the toy model, we observed that the rank-one RNN was able to eventually escape the oscillations and decrease the loss further. Studying the learned latent circuit revealed that the escape was accompanied with a sharpening of the curvature around the ghost (Fig. 3A), whereas our toy model had a fixed curvature regardless of r . With the increased curvature, $\kappa(t)$ spent less time in uncertain states around κ^* and the output abruptly transitioned between the two states. Though prior work has shown that networks with many parameters are more expressive compared to their counterparts [31], this observa-

tion suggests an added benefit: They may have desirable loss landscapes to achieve the global minima, which may exist, but remain unattainable, in less expressive models.

Next, we investigated the mechanism behind our finding that high learning rates prevented learning altogether in these RNNs (Fig. S1). Specifically, we examined the latent circuit evolution in an RNN trained with a high learning rate (Fig. 3B). Similar to our toy model, the network underwent a saddle-node bifurcation and remained stuck in a no-learning zone with a nearly zero gradient. Though one might think that the fixed nature of the output confidence was the reason, we observed that another network, in which c was trainable, still got stuck in the no-learning zone (data not shown; code available via Zenodo). In contrast, we found that artificially lowering the confidence levels allowed the RNNs to become unstuck and re-learn the task (Fig. 4). This is in line with the toy model’s predictions, in which lower confidence values enable small, yet non-zero, gradients to form beyond the point of no return (Fig. 2A). Taken together, these findings highlight the importance of implementing mechanisms beyond loss minimization (*e.g.*, see simulated annealing [48]) to lower confidence levels when learning stalls in biological and artificial networks.

Finally, we tested whether our observations with rank-one RNNs would generalize to their full-rank counterparts, and/or whether increasing the network’s resources (*e.g.*, number of ranks, following the first optimization strategy outlined above) could help stabilize learning dynamics. Since additional ranks are not necessary to solve the task, inspired by sloppy parameters in physics [49], we call these as “sloppy ranks.” As shown in Figure S2, increasing the number of trainable ranks in W consistently

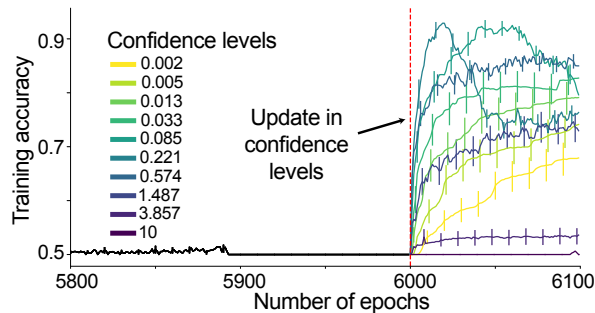


FIG. 4. **Lowering the confidence allows RNNs to recover from the no-learning zone.** We trained 100 RNNs with a confidence $c = 10$ and the learning rate $\alpha = 0.02$ for 6000 epochs, otherwise using the same parameters as in Fig. 3. Out of 100, 74 RNNs learned the task at some point, whereas 54 of them entered the no-learning zone (quantified as having training accuracy of ≤ 0.5 for the last 50 epochs). We further trained these RNNs after lowering the confidence levels, which allowed them to recover. Solid lines: means. Error bars: s.e.m. over 54 networks.

resulted in learning with fewer epoch. Notably, for low-rank RNNs showed the rapid decrease of the loss function within few epochs. In contrast, for full-rank RNNs, we observed gradual decreases across extended epochs (Figure S2). However, even full-rank RNNs still exhibited oscillatory phases and occasionally became stuck in no-learning zones. Therefore, while utilizing sloppy ranks for learning did partially stabilize and speed up the learning (naively, making strategy (1) more desirable than strategy (2) if the resources are not scarce), an additional mechanism of lowering confidence levels may still be necessary to prevent getting trapped in no-learning zones.

Overall, the toy model we introduced in this work is a simple, powerful, and analytically tractable example. By closely examining the training process of this model, we replicated complex learning dynamics that are also observed in practice. Our findings suggest that these complex learning dynamics, typically associated with deep architectures and complicated tasks [45], can originate from the optimization process itself and be observed in low-dimensional systems performing simple tasks when parameters are learned via loss minimization, rather than tuned. Similar challenges have been noted in the deep learning literature, such as the “catapult mechanism” [50] and “pathological curvature” [51]. Thus, our toy model provides a simple and analytically tractable starting point for exploring potential remedies. Moreover, our analyses with rank-one RNNs suggest an alternative, bifurcation-free, mechanism for abrupt learning. By studying the latent circuits during learning, we identified the emergence of ghost points as the precursors of the stereotypical trajectories that RNNs developed to solve the DA task. While prior work has examined these latent circuits in fully trained low-rank RNNs [28–31], our find-

ings here highlight the distinct advantages of studying latent circuits during task training, *i.e.*, for investigating the full window of learning dynamics.

Finally, our findings may have potential implications for research in biophysics and neuroscience. First, sloppy dimensions are universally observed in many physical models [49]. Our findings suggest that one reason for their existence may be the need to stabilize the learning dynamics of few well-constrained dimensions. Second, in the traditional deep learning paradigm, the confidence levels would be optimized, not artificially controlled, and therefore the training process would be susceptible to no-learning zones. We presented a potential remedy in Fig. 4, *i.e.*, different mechanisms may be crucial for learning (practicing) versus inference (performing). This observation mirrors seminal work on adult zebra finch, where males exhibit variability during practice, but perform with precision and reduced neural variability in the presence of a female [52, 53]. Therefore, our theoretical observations of no-learning zones and their dependency on confidence levels constitute biologically testable predictions about the nature of learning.

Code availability—The code used to support the findings of the study is available at <https://doi.org/10.5281/zenodo.13686989>

Acknowledgements—We would like to thank Dr. Marta Blanco-Pozo and Dr. Saeed Ahmed Khan for their insightful comments on the manuscript, Dr. Nina Milolane, Abby Bertics and members of the Geometric Intelligence Lab for their helpful feedback on an earlier version of the project, and Dr. Boris Shraiman for fruitful discussions on the sloppy dimensions and learning in high-dimensional dynamical systems. MJS gratefully acknowledges funding from the Simons Collaboration on the Global Brain, the Vannevar Bush Faculty Fellowship Program of the U.S. Department of Defense, and Howard Hughes Medical Institute. FD receives funding from Stanford University’s Mind, Brain, Computation and Technology program, which is supported by the Stanford Wu Tsai Neuroscience Institute. FD expresses gratitude for the valuable mentorship he received at PHI Lab during his internship at NTT Research. EC’s internship was supported in part by a grant from the Feldman-McClelland Open-a-Door fund of the Pittsburgh Foundation. Some of the computing for this project was performed on the Sherlock cluster. We would like to thank Stanford University and the Stanford Research Computing Center for providing computational resources and support that contributed to these research results.

* Co-first authors

† Co-supervision

[1] Donald Olding Hebb. *The organization of behavior: A*

- neuropsychological theory*. Psychology press, 2005.
- [2] Eric R Kandel, James H Schwartz, Thomas M Jessell, Steven Siegelbaum, A James Hudspeth, Sarah Mack, et al. *Principles of neural science*, volume 4. McGraw-hill New York, 2000.
 - [3] Anne E Urai, Brent Doiron, Andrew M Leifer, and Anne K Churchland. Large-scale neural recordings call for new insights to link brain and behavior. *Nature neuroscience*, 25(1):11–19, 2022.
 - [4] Logan G Wright, Tatsuhiro Onodera, Martin M Stein, Tianyu Wang, Darren T Schachter, Zoey Hu, and Peter L McMahon. Deep physical neural networks trained with backpropagation. *Nature*, 601(7894):549–555, 2022.
 - [5] Peter L McMahon. The physics of optical computing. *Nature Reviews Physics*, 5(12):717–734, 2023.
 - [6] Sunil Pai, Zhanghao Sun, Tyler W Hughes, Taewon Park, Ben Bartlett, Ian AD Williamson, Momchil Minkov, Maziyar Milanizadeh, Nathnael Abebe, Francesco Morichetti, et al. Experimentally realized in situ backpropagation for deep learning in photonic neural networks. *Science*, 380(6643):398–404, 2023.
 - [7] Demis Hassabis, Dharsan Kumaran, Christopher Summerfield, and Matthew Botvinick. Neuroscience-inspired artificial intelligence. *Neuron*, 95(2):245–258, 2017.
 - [8] Anthony M Zador. A critique of pure learning and what artificial neural networks can learn from animal brains. *Nature communications*, 10(1):3770, 2019.
 - [9] Lukas Eisenmann, Zahra Monfared, Niclas Göring, and Daniel Durstewitz. Bifurcations and loss jumps in rnn training. *Advances in Neural Information Processing Systems*, 36, 2024.
 - [10] Udith Haputhanthri, Liam Storan, Yiqi Jiang, Adam Shai, Hakki Orhun Akengin, Mark Schnitzer, Fatih Dinc, and Hidenori Tanaka. Why do recurrent neural networks suddenly learn? bifurcation mechanisms in neuro-inspired short-term memory tasks. In *ICML 2024 Workshop on Mechanistic Interpretability*, 2024.
 - [11] Peter DelMastro, Rushiv Arora, Edward Rietman, and Hava T Siegelmann. On the dynamics of learning time-aware behavior with recurrent neural networks. *arXiv preprint arXiv:2306.07125*, 2023.
 - [12] Aarohi Srivastava, Abhinav Rastogi, Abhishek Rao, Abu Awal Md Shoeb, Abubakar Abid, Adam Fisch, Adam R Brown, Adam Santoro, Aditya Gupta, Adrià Garriga-Alonso, et al. Beyond the imitation game: Quantifying and extrapolating the capabilities of language models. *arXiv preprint arXiv:2206.04615*, 2022.
 - [13] Sanjeev Arora and Anirudh Goyal. A theory for emergence of complex skills in language models. *arXiv preprint arXiv:2307.15936*, 2023.
 - [14] Dingli Yu, Simran Kaur, Arushi Gupta, Jonah Brown-Cohen, Anirudh Goyal, and Sanjeev Arora. Skill-mix: A flexible and expandable family of evaluations for ai models. *arXiv preprint arXiv:2310.17567*, 2023.
 - [15] Ekdeep Singh Lubana, Kyogo Kawaguchi, Robert P Dick, and Hidenori Tanaka. A percolation model of emergence: Analyzing transformers trained on a formal language. *arXiv preprint arXiv:2408.12578*, 2024.
 - [16] Maya Okawa, Ekdeep S Lubana, Robert Dick, and Hidenori Tanaka. Compositional abilities emerge multiplicatively: Exploring diffusion models on a synthetic task. *Advances in Neural Information Processing Systems*, 36, 2023.
 - [17] Jason Wei, Yi Tay, Rishi Bommasani, Colin Raffel, Barret Zoph, Sebastian Borgeaud, Dani Yogatama, Maarten Bosma, Denny Zhou, Donald Metzler, et al. Emergent abilities of large language models. *arXiv preprint arXiv:2206.07682*, 2022.
 - [18] Jordan Hoffmann, Sebastian Borgeaud, Arthur Mensch, Elena Buchatskaya, Trevor Cai, Eliza Rutherford, Diego de Las Casas, Lisa Anne Hendricks, Johannes Welbl, Aidan Clark, et al. An empirical analysis of compute-optimal large language model training. *Advances in Neural Information Processing Systems*, 35:30016–30030, 2022.
 - [19] Alethea Power, Yuri Burda, Harri Edwards, Igor Babuschkin, and Vedant Misra. Grokking: Generalization beyond overfitting on small algorithmic datasets, 2022.
 - [20] Razvan Pascanu, Tomas Mikolov, and Yoshua Bengio. On the difficulty of training recurrent neural networks. In *International conference on machine learning*, pages 1310–1318. Pmlr, 2013.
 - [21] Kenji Doya et al. Bifurcations in the learning of recurrent neural networks 3. *learning (RTRL)*, 3:17, 1992.
 - [22] Ian J Goodfellow, Oriol Vinyals, and Andrew M Saxe. Qualitatively characterizing neural network optimization problems. *arXiv preprint arXiv:1412.6544*, 2014.
 - [23] Gautam Reddy. The mechanistic basis of data dependence and abrupt learning in an in-context classification task. In *The Twelfth International Conference on Learning Representations*, 2023.
 - [24] Catherine Olsson, Nelson Elhage, Neel Nanda, Nicholas Joseph, Nova DasSarma, Tom Henighan, Ben Mann, Amanda Askell, Yuntao Bai, Anna Chen, et al. In-context learning and induction heads. *arXiv preprint arXiv:2209.11895*, 2022.
 - [25] David Sussillo and Omri Barak. Opening the black box: low-dimensional dynamics in high-dimensional recurrent neural networks. *Neural computation*, 25(3):626–649, 2013.
 - [26] Valerio Mante, David Sussillo, Krishna V Shenoy, and William T Newsome. Context-dependent computation by recurrent dynamics in prefrontal cortex. *nature*, 503(7474):78–84, 2013.
 - [27] Guangyu Robert Yang, Madhura R Joglekar, H Francis Song, William T Newsome, and Xiao-Jing Wang. Task representations in neural networks trained to perform many cognitive tasks. *Nature neuroscience*, 22(2):297–306, 2019.
 - [28] Alexis Dubreuil, Adrian Valente, Manuel Beiran, Francesca Mastrogiuseppe, and Srdjan Ostojic. The role of population structure in computations through neural dynamics. *Nature Neuroscience*, pages 1–12, 2022.
 - [29] Adrian Valente, Jonathan W Pillow, and Srdjan Ostojic. Extracting computational mechanisms from neural data using low-rank rnns. *Advances in Neural Information Processing Systems*, 35:24072–24086, 2022.
 - [30] Francesca Mastrogiuseppe and Srdjan Ostojic. Linking connectivity, dynamics, and computations in low-rank recurrent neural networks. *Neuron*, 99(3):609–623, 2018.
 - [31] Manuel Beiran, Alexis Dubreuil, Adrian Valente, Francesca Mastrogiuseppe, and Srdjan Ostojic. Shaping dynamics with multiple populations in low-rank recurrent networks. *Neural Computation*, 33(6):1572–1615, 2021.
 - [32] Friedrich Schuessler, Francesca Mastrogiuseppe, Alexis Dubreuil, Srdjan Ostojic, and Omri Barak. The inter-

- play between randomness and structure during learning in rnns. *Advances in neural information processing systems*, 33:13352–13362, 2020.
- [33] Florian Hess, Zahra Monfared, Manuel Brenner, and Daniel Durstewitz. Generalized teacher forcing for learning chaotic dynamics. In *Proceedings of the 40th International Conference on Machine Learning, ICML’23*. JMLR.org, 2023.
- [34] Antônio H Ribeiro, Koen Tiels, Luis A Aguirre, and Thomas Schön. Beyond exploding and vanishing gradients: analysing rnn training using attractors and smoothness. In *International conference on artificial intelligence and statistics*, pages 2370–2380. PMLR, 2020.
- [35] Niru Maheswaranathan, Alex Williams, Matthew Golub, Surya Ganguli, and David Sussillo. Reverse engineering recurrent networks for sentiment classification reveals line attractor dynamics. *Advances in neural information processing systems*, 32, 2019.
- [36] Niru Maheswaranathan, Alex Williams, Matthew Golub, Surya Ganguli, and David Sussillo. Universality and individuality in neural dynamics across large populations of recurrent networks. *Advances in neural information processing systems*, 32, 2019.
- [37] Steven H Strogatz. *Nonlinear dynamics and chaos: with applications to physics, biology, chemistry, and engineering*. CRC press, 2018.
- [38] Dominik Schmidt, Georgia Koppe, Zahra Monfared, Max Beutelspacher, and Daniel Durstewitz. Identifying nonlinear dynamical systems with multiple time scales and long-range dependencies. In *International Conference on Learning Representations*, 2021.
- [39] Robert Haschke and Jochen J. Steil. Input space bifurcation manifolds of recurrent neural networks. *Neurocomputing*, 64:25–38, 2005. Trends in Neurocomputing: 12th European Symposium on Artificial Neural Networks 2004.
- [40] Alexander Rehmer and Andreas Kroll. The effect of the forget gate on bifurcation boundaries and dynamics in recurrent neural networks and its implications for gradient-based optimization. In *2022 International Joint Conference on Neural Networks (IJCNN)*, pages 01–08, 2022.
- [41] Viktor Avrutin, Michael Schanz, and Soumitro Banerjee. Occurrence of multiple attractor bifurcations in the two-dimensional piecewise linear normal form map. *Nonlinear Dynamics*, 67:293–307, 2012.
- [42] Anindita Ganguli and Soumitro Banerjee. Dangerous bifurcation at border collision: When does it occur? *Physical Review E—Statistical, Nonlinear, and Soft Matter Physics*, 71(5):057202, 2005.
- [43] Z. Monfared and D. Durstewitz. Existence of n-cycles and border-collision bifurcations in piecewise-linear continuous maps with applications to recurrent neural networks. *Nonlinear Dynamics*, 101(2):1037–1052, Jul 2020.
- [44] Matthew D Golub and David Sussillo. Fixedpointfinder: A tensorflow toolbox for identifying and characterizing fixed points in recurrent neural networks. *Journal of Open Source Software*, 3(31):1003, 2018.
- [45] Hao Li, Zheng Xu, Gavin Taylor, Christoph Studer, and Tom Goldstein. Visualizing the loss landscape of neural nets. *Advances in neural information processing systems*, 31, 2018.
- [46] David Sussillo and Larry F Abbott. Generating coherent patterns of activity from chaotic neural networks. *Neuron*, 63(4):544–557, 2009.
- [47] Fatih Dinc, Adam Shai, Mark Schnitzer, and Hide-nori Tanaka. Cornn: Convex optimization of recurrent neural networks for rapid inference of neural dynamics. *Advances in Neural Information Processing Systems*, 36:51273–51301, 2023.
- [48] Scott Kirkpatrick, C Daniel Gelatt Jr, and Mario P Vecchi. Optimization by simulated annealing. *science*, 220(4598):671–680, 1983.
- [49] Ryan N Gutenkunst, Joshua J Waterfall, Fergal P Casey, Kevin S Brown, Christopher R Myers, and James P Sethna. Universally sloppy parameter sensitivities in systems biology models. *PLoS computational biology*, 3(10):e189, 2007.
- [50] Aitor Lewkowycz, Yasaman Bahri, Ethan Dyer, Jascha Sohl-Dickstein, and Guy Gur-Ari. The large learning rate phase of deep learning: the catapult mechanism. *arXiv preprint arXiv:2003.02218*, 2020.
- [51] James Martens et al. Deep learning via hessian-free optimization. In *Icml*, volume 27, pages 735–742, 2010.
- [52] Neal A Hessler and Allison J Doupe. Social context modulates singing-related neural activity in the songbird forebrain. *Nature neuroscience*, 2(3):209–211, 1999.
- [53] Mimi H Kao, Brian D Wright, and Allison J Doupe. Neurons in a forebrain nucleus required for vocal plasticity rapidly switch between precise firing and variable bursting depending on social context. *Journal of Neuroscience*, 28(49):13232–13247, 2008.
- [54] Adam Paszke, Sam Gross, Soumith Chintala, Gregory Chanan, Edward Yang, Zach DeVito, Zeming Lin, Alban Desmaison, Luca Antiga, and Adam Lerer. Automatic differentiation in pytorch. In *31st Conference on Neural Information Processing Systems*, 2017.

End Matter

Derivations of the toy model results

In this section, we perform the analytical derivations of the toy model we introduced in the main text in the limit $c \rightarrow \infty$ such that the toy model output takes the form:

$$\hat{o}(x(t)) = \Theta(x(t) - x^*), \quad (6)$$

for some pre-defined $x^* > 0$, where $\Theta(x)$ is Heaviside function with $\Theta(x) = 1$ if $x > 0$, and zero otherwise. Using this output, for $r < 0$, the loss function in Eq. (1) is trivially T , since the model output is always 0. Therefore, we will focus on the case with $r > 0$.

Since the toy model has a simple quadratic form, we can compute $x(t)$ as a function of time t , with the initial condition $x(0) = 0$. After straightforward algebra, $x(t)$ becomes:

$$x(t) = \begin{cases} \sqrt{r} \tan(\sqrt{r}t) & \text{for } t \leq t^*, \\ \infty & \text{otherwise,} \end{cases} \quad (7)$$

where we define $t^* = \frac{\pi}{2\sqrt{r}}$ as the escape time for which $x(t^*) \rightarrow \infty$. In the limit $x^* \rightarrow \infty$, we will simply assume that the network output is 0 before the escape, *e.g.*, $t \leq t^*$, and 1 after the escape, *e.g.*, $t \geq t^*$. Using this, we can explicitly compute the loss function:

$$\begin{aligned} \mathcal{L}(r) &= \int_0^{2T} dt (\hat{o}(t) - o(t))^2, \\ &= \int_0^T dt (\hat{o}(t))^2 + \int_T^{2T} dt (\hat{o}(t) - 1)^2. \end{aligned} \quad (8)$$

There are three important regimes here: i) $t^* \leq T$, ii) $T \leq t^* \leq 2T$, and iii) $2T \leq t^*$. Let us start with the first case, $t^* \leq T$:

$$\begin{aligned} \mathcal{L}(r) &= \underbrace{\int_0^{t^*} dt (\hat{o}(t))^2}_0 + \int_{t^*}^T dt (\hat{o}(t))^2 + \underbrace{\int_T^{2T} dt (\hat{o}(t) - 1)^2}_0 \\ &= \int_{t^*}^T dt = T - t^* = T - \frac{\pi}{2\sqrt{r}}, \quad \text{for } r \geq \frac{\pi^2}{4T^2} \end{aligned} \quad (9)$$

Next, we consider the second case, $T \leq t^* \leq 2T$:

$$\begin{aligned} \mathcal{L}(r) &= \underbrace{\int_0^T dt (\hat{o}(t))^2}_0 + \underbrace{\int_{t^*}^{2T} dt (\hat{o}(t) - 1)^2}_0 + \int_T^{t^*} dt (\hat{o}(t) - 1)^2 \\ &= \int_T^{t^*} dt = \frac{\pi}{2\sqrt{r}} - T, \quad \text{for } \frac{\pi^2}{16T^2} \leq r \leq \frac{\pi^2}{4T^2} \end{aligned} \quad (10)$$

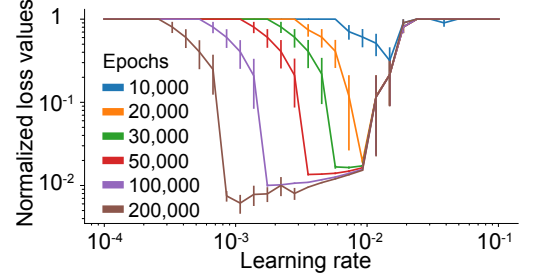


FIG. S1. We performed the analysis in Fig. 2D for the rank-one RNNs trained on the DA task. Parameters: $\tau = 10ms$, $\Delta t = 5ms$, $T = 100ms$, $N = 100$ neurons, $c = 10$. We initialized all units to be $x(0) = -0.3$ and used stochastic gradient descent.

Finally, we consider the case $t^* \geq 2T$:

$$\begin{aligned} \mathcal{L}(r) &= \underbrace{\int_0^T dt (\hat{o}(t))^2}_0 + \int_T^{2T} dt (\hat{o}(t) - 1)^2, \\ &= T. \end{aligned} \quad (11)$$

Bringing all cases together, we find the loss function:

$$\mathcal{L}(r) = \begin{cases} \left| T - \frac{\pi}{2\sqrt{r}} \right| & \text{for } r \geq \frac{\pi^2}{16T^2} = \frac{r^*}{4}, \\ T & \text{otherwise.} \end{cases} \quad (12)$$

When $r^* = \frac{\pi^2}{4T^2}$, this loss function is zero, achieving the global optimum.

An important observation is that there is a kink at the optimal value, $r^* = \frac{\pi^2}{4T^2}$. This means that the gradient is never truly zero, even when the loss function is zero. To see this, let us compute the gradient of the loss function:

$$\frac{d\mathcal{L}}{dr} = \begin{cases} -\frac{\pi}{4r^{3/2}} & \text{for } \frac{\pi^2}{16T^2} < r < \frac{\pi^2}{4T^2}, \\ \frac{\pi}{4r^{3/2}} & \text{for } r > \frac{\pi^2}{4T^2}, \\ 0 & \text{for } r < \frac{\pi^2}{16T^2}. \end{cases} \quad (13)$$

The derivative at $r = r^* = \frac{\pi^2}{4T^2}$ becomes:

$$\text{At } r = \frac{\pi^2}{4T^2} : \quad \frac{d\mathcal{L}}{dr} = \begin{cases} -\frac{2T^3}{\pi^2} & \text{from the left,} \\ \frac{2T^3}{\pi^2} & \text{from the right.} \end{cases} \quad (14)$$

Now, with a learning rate α^* , the model would be thrown from the global minimum to the point of no return boundary and get stuck in the no-learning zone during the oscillations if it receives the following update:

$$\alpha^* \left. \frac{d\mathcal{L}}{dr} \right|_{r \rightarrow r^*+} = \frac{3}{4} r^* = \frac{3\pi^2}{16T^2} \implies \alpha^* = \frac{3\pi^4}{32} T^{-5}. \quad (15)$$

Any $\alpha \geq \alpha^* \sim O(T^{-5})$, the model would eventually pass the point of no return and output only zeros. For Fig. 2 with $T = 100$, this corresponds to roughly $9 * 10^{-10}$.

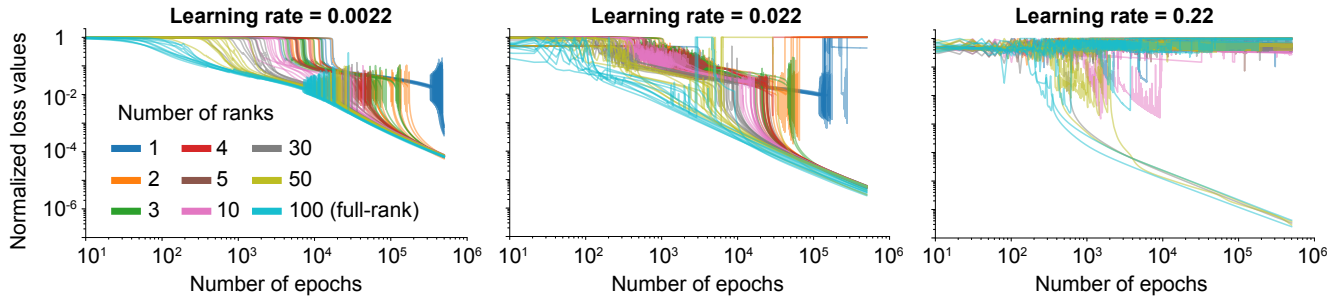


FIG. S2. **Increasing the ranks of the RNNs available for training partially stabilized learning dynamics.** We trained RNNs with varying ranks (1, 2, 3, 4, 5, 10, 30, 50, 100) on the DA task. The output of each RNN was defined as $\hat{o}(r) = \sigma(w_{\text{out}}^T r + b_{\text{out}})$, where, w_{out} and b_{out} are output weights and biases, respectively. *Left.* The RNN trained with a relatively low learning rate showed the abrupt jump in the loss function values and the following oscillations, similar to Fig. 3A. Increasing the number of trainable ranks shortened the learning process, with milder and sustained decreases in the loss function, but still substantial oscillations. *Middle.* When training the same networks with higher learning rates, we observed occasional entrance to no-learning zones (with negligible gradients). *Right.* For a substantially high learning rate, few RNNs that could train without entering the no-learning zone had either 50 or 100 available ranks. Parameters: $\tau = 10ms$, $\Delta t = 5ms$, $T = 100ms$, and $N = 100$ neurons. We initialized all units to be $x(0) = -0.3$ and used stochastic gradient descent. Each line corresponds to a run with a different seed.

Analysis with recurrent neural networks

For the RNN model described in the main text, we set $\kappa^* = 1$ and $c = 10$ in our experiments. Practically, we defined a Pytorch model [54] and performed minimization with a stochastic gradient descent, using a single trial, where all neurons are initialized with $x(0) = -0.3$.

There are several important distinctions between the trained RNNs and our toy model. First, for large κ , the time evolution equations asymptotically becomes:

$$\tau \dot{\kappa}(t) \rightarrow -\kappa(t) + O(1), \quad |\kappa| \rightarrow \infty, \quad (16)$$

where $O(1)$ refers to the κ independent saturation term due to the saturation of $\tanh(\cdot)$ non-linearities. Thus, unlike the toy model, RNN equations cannot generate a global ghost point, as there is always at least one fixed point to accommodate $f(\kappa; m, n, b) \rightarrow -\kappa$ limit as $\kappa \rightarrow \pm\infty$. Instead, as we show in Fig. 3, the ghost point emerges locally.

Second, the RNN equations have a characteristic time-scale, τ , with respect to which we perform an Euler discretization and design the delay period T . Specifically, we pick $\Delta t = 5ms$ such that $\Delta = \Delta t / \tau = 0.5$ and the time evolution equations become:

$$x[t + \Delta t] = (1 - \Delta)x[t] + \Delta \tanh(Wx[t] + b). \quad (17)$$

Finally, the rank-one RNN, despite being characterized by a single dynamical variable, has $O(N)$ parameters. This means there are far more knobs to turn, effectively creating redundancy and sloppy dimensions. Thus, we do not expect the critical learning rate in RNNs to follow Eq. (15), as the RNNs are more expressive than the toy model. For example, they can learn to change the curvature of the ghost point as shown in Fig. 3A. But, as shown in Fig. S1, we did recover the same trend between the learning rates and the final loss function values.

For our analysis with increasing ranks in Fig. S2, we used the RNNs described by Eq. (3), but with the following output:

$$\hat{o}(t) = w_{\text{out}}^T x(t) + b_{\text{out}}, \quad (18)$$

where $w_{\text{out}} \in \mathbb{R}^N$ and $b_{\text{out}} \in \mathbb{R}$ are trainable parameters. Unlike the rank-one RNNs, this choice allows to train the confidence parameter (c for the previous models) and the threshold value (κ^* or x^* for previous models). We enforce the rank constraints by defining $M \in \mathbb{R}^{N \times K}$ and $N \in \mathbb{R}^{K \times N}$ such that

$$W = MN \quad (19)$$

is a low-rank matrix. We train these networks by first computing the forward evolution using the same discretization procedure explained in Eq. (17) and performing stochastic gradient descent on the discretized version of the loss function in Eq. (1).